THEORY AND DESIGN OF UNIFORM CONCENTRIC SPHERICAL ARRAYS WITH FREQUENCY INVARIANT CHARACTERISTICS

S. C. Chan and H. H. Chen
Department of Electrical and Electronic Engineering
The University of Hong Kong, Pokfulam Road, Hong Kong

***Abstract*—**This paper proposes a new digital beamformer for uniform concentric spherical array (UCSA) having nearly frequency invariant (FI) characteristics. The basic principle is to transform the received signals to the phase mode and remove the frequency dependency of the individual phase mode through the use of a digital beamforming network. It is shown that the far field pattern of the array is determined by a set of weights and it is approximately invariant over a wide range of frequencies. FI UCSAs are electronic steerable in both the azimuth angle and elevation angle, unlike their concentric circular array counterpart. A design example is given to demonstrate the design and performance of the proposed FI UCSA.

I. INTRODUCTION

Beamforming using sensor arrays is an effective method for suppressing interferences whose angles of arrival are different from the desired looking direction. They find important applications in sonar, radar, acoustics, and radio communications [1]-[3]. Traditional adaptive broadband beamformer usually employs tapped-delay lines or linear transversal filters with adaptive coefficients to generate appropriate beam patterns for suppressing undesirable interference. This usually requires considerable number of adaptive coefficients resulting in a rather long convergence time and high implementation complexity. These problems can be remedied by using subband decomposition technique, partial adaptation or using frequency invariant beamformers (FIB) [4]-[6], [8]. In FIBs, a beam-forming network is used to generate beam pattern with approximately frequency invariant (FI) characteristics over the frequency band of interest. They can attenuate broadband directional interference using an adaptive beamformer with very few number of adaptive filter coefficients [4]. One of the widely studied FIB is the uniform linear array (ULA) FIB [4]-[7]. Due to the geometry of ULA, its angular resolution at boresight is better than that at its end-fire. In addition, it allows many efficient direction-of-arrival (DOA) detection algorithms to be developed. For example, the MUSIC algorithm [9] provides a high resolution method for detecting the angle of arrival (AoA) of the signal sources based on the subspace approach. The MUSIC algorithm is also applicable to DOA estimation of wideband coherent sources by performing the algorithm in beamspace using ULA-FIB [8]. Besides AoA estimation of wideband sources, adaptive interference suppression using beamspace adaptive beamforming [4] is also very attractive because of the small number of adaptive coefficients required and the possibility of employing partial adaptation, yielding faster convergence and fewer number of high speed variable multipliers.

Recently, electronic steerable uniform-circular arrays (UCAs) [10] with frequency invariant characteristics were studied in [11]. Unfortunately, the passband of a UCA is rather narrow because it is closely related to the radius of the array. To obtain a frequency invariant characteristic over a larger bandwidth, uniform concentric circular arrays (UCCA) are proposed in [12] and [13]. The basic idea of the FI UCCA is to transform each snapshot sampled by the array to the phase modes via an Inverse Discrete Fourier Transform (IDFT). The transformed data is then filtered to compensate for the frequency dependence of the phase modes. Finally, these frequency invariant phase-modes are linear combined using a set of weights or coefficients to obtain the desired frequency invariant beam patterns. These weights, which govern the far field pattern of the UCCA, can be designed by conventional 1D digital filter design techniques. Alternatively, these coefficients can be varied by an adaptive algorithm to form an adaptive beamformer with approximately frequency invariant characteristics. The compensation filters in the fixed beamforming network are designed using second order cone programming (SOCP) [14][15]. Due to the geometry of the UCCA, the beampattern is not arbitrarily steerable with respect to the elevation angle. To overcome these disadvantages, we study in this paper the design of a uniform concentric spherical array (UCSA) with frequency invariant (FI) characteristics. The UCSA-FIB has all the advantages of the UCCA mentioned above while possessing electronically steerable characteristic and uniform beampattern in both the azimuth and elevation angles. These characteristics make it more suitable than the UCCA in two dimensional DOA estimation and spatial-time beamforming.

The paper is organized as follows: In section II, the structure of the UCSA is introduced. The design of the FI UCSA is presented in section III. A design example is given in section IV and conclusions are drawn in section V.

II. UNIFORM CONCENTRIC SPHERICAL ARRAY (UCSA)

The UCSA proposed in this paper is constructed from a series of vertical UCCAs, which are uniformly distributed along the azimuth angle as shown in Figure 1. Each UCCA is composed of P rings and each ring has K_p omnidirectional sensors located at $\{r_p\cos\phi_{k_p^{(\phi)}}, r_p\sin\phi_{k_p^{(\phi)}}\}$ (represented as Cartesian Coordinate with the center as the origin) where r_p is the radius of the p^{th} ring, $p=1,\cdots,P$, $\phi_{k_p^{(\phi)}}=2\pi k_p^{(\phi)}/K_p^{(\phi)}$ and $k_p^{(\phi)}=0,\cdots,K_p^{(\phi)}-1$ as shown in Figure 2. In UCCAs, the inter-sensor spacing in each ring is fixed at $\lambda/2$ where λ is the smallest wavelength of the array to be operated and is denoted by λ_s. The radius of the p^{th} ring of the UCCA is given by

$$r_p=\lambda_s/(4\sin(\pi/K_p^{(\phi)})). \tag{1}$$

For convenience, this radius is represented as its normalized version $\hat{r}_p=r_p/\lambda_s=1/(4\sin(\pi/K_p^{(\phi)}))$. Let α denote the ratio of the sampling frequency f_s to the maximum frequency $f_{\max}$ ($\alpha=f_s/f_{\max}$), the phase difference between the $k_p^{(\phi)th}$ sensor and the center of the UCCA is $\chi_{k_p^{(\phi)}}=2\pi\hat{r}_p\alpha\sin\theta\cos(\phi-\phi_{k_p^{(\phi)}})$, and the corresponding phase shift is $e^{j\omega\hat{r}_p\alpha\sin\theta\cos(\phi-\phi_{k_p^{(\phi)}})}$, where ϕ, and θ are the azimuth angle and the elevation angle respectively, as shown in Figure 3. Hence, the steering vector [1] of the p^{th} ring of a UCCA is:

$$\boldsymbol{s}_p^{(\phi)}=[e^{j\omega\hat{r}_p\alpha\sin\theta\cos(\phi-\phi_0)}\ \cdots\ e^{j\omega\hat{r}_p\alpha\sin\theta\cos(\phi-\phi_{K_p^{(\phi)}-1})}]. \tag{2}$$

The azimuth angle ϕ is on the horizontal plane where the sensors are situated. It measures from a reference imaginary

axis on this horizontal plane, while the elevation angle θ is measured from a reference imaginary axis perpendicular to the horizontal plane. To obtain a UCSA, each ring of the UCCA is rotated by $\theta_{k_p^{(\theta)}}$ angle, $\theta_{k_p^{(\theta)}} = 2\pi k_p^{(\theta)} / K_p^{(\theta)}$, $k_p^{(\theta)} = 0, \cdots, K_p^{(\theta)} - 1$. The geometry of the UCSA obtained by this way is shown in Figure 3. Based on the UCCA described above, the steering vector of the $k_p^{(\theta)th}$ ring can be written as:

$$\boldsymbol{s}_{k_p^{(\theta)}} = [e^{j\omega\hat{r}_p \sin(\theta+(\frac{\pi}{2}-\theta_{k_p^{(\theta)}}))\cos(\phi-\phi_0)} \quad \cdots \quad e^{j\omega\hat{r}_p \sin(\theta+(\frac{\pi}{2}-\theta_{k_p^{(\theta)}}))\cos(\phi-\phi_{k_p^{(\phi)}})}]. \tag{3}$$

It can be written in a more concise form:

$$\boldsymbol{s}_{k_p^{(\theta)}} = [e^{j\omega\hat{r}_p \cos(\theta-\theta_{k_p^{(\theta)}})\cos(\phi-\phi_0)} \quad \cdots \quad e^{j\omega\hat{r}_p \cos(\theta-\theta_{k_p^{(\theta)}})\cos(\phi-\phi_{k_p^{(\phi)}})}]. \tag{4}$$

III. FREQUENCY INVARIANT (FI) UCSAS

Figure 4 shows the structure of the broadband FIB for the p^{th} sphere of a UCSA. After appropriate down-converting, lowpass filtering and sampling, the sampled signals from the antennas are given by the matrix $\boldsymbol{X}_p[n]$ with $[X_p[n]]_{k_p^{(\phi)},k_p^{(\theta)}} = x_{k_p^{(\phi)},k_p^{(\theta)}}[n]$, which is called a snapshot at sampling instance *n*. This snapshot is 2D-IDFT transformed to the phase-mode and the transformed snapshot is denoted by an $M_p^{(\phi)} \times M_p^{(\theta)}$ matrix $\boldsymbol{V}_p[n]$, and

$$[\boldsymbol{V}_p[n]]_{m_p^{(\phi)},m_p^{(\theta)}} = v_{m_p^{(\phi)},m_p^{(\theta)}}[n] \tag{5}$$
$$= \sum_{k_p^{(\theta)}=0}^{K_p^{(\theta)}-1} \sum_{k_p^{(\phi)}=0}^{K_p^{(\phi)}-1} x_{k_p^{(\phi)},k_p^{(\theta)}}[n] e^{j\frac{2\pi k_p^{(\phi)} m_p^{(\phi)}}{K_p^{(\phi)}}} e^{j\frac{2\pi k_p^{(\theta)} m_p^{(\theta)}}{K_p^{(\theta)}}}.$$

Here, $[\mathbf{A}]_{m,n}$ denotes the (*m*,*n*) entry of matrix **A**. We assume that $M_p^{(\phi)}$ and $M_p^{(\theta)}$ are odd numbers and define $L_p^{(i)} = (M_p^{(i)} - 1)/2$, $i = \phi, \theta$. Each branch of the 2D-IDFT output is then filtered by $H_{m_p^{(\phi)},m_p^{(\theta)}}(\omega)$ (to compensate for the frequency dependency as we shall see later in this section), multiplied with $g_{m_p^{(\phi)},m_p^{(\theta)}}$ before combining to give the beamformer output $y_p[n]$:

$$y_p[n] = \sum_{m_p^{(\theta)}=-L_p^{(\theta)}}^{L_p^{(\theta)}} \sum_{m_p^{(\phi)}=-L_p^{(\phi)}}^{L_p^{(\phi)}} \left(v_{m_p^{(\phi)},m_p^{(\theta)}}[n] * h_{m_p^{(\phi)},m_p^{(\theta)}}[n] \right) \cdot g_{m_p^{(\phi)},m_p^{(\theta)}} \tag{6}$$

where * denotes discrete-time convolution. To obtain the spatial-temporal transfer function of the beamformer, let us assume that there is only one source signal $s(n)$ with spectrum $S(\omega)$. Taking the Discrete Time Fourier Transform (DTFT) of equation (5), one gets

$$V_{m_p^{(\phi)},m_p^{(\theta)}}(\omega) = \sum_{k_p^{(\theta)}=0}^{K_p^{(\theta)}-1} \sum_{k_p^{(\phi)}=0}^{K_p^{(\phi)}-1} X_{k_p^{(\phi)},k_p^{(\theta)}}(\omega) e^{j\frac{2\pi k_p^{(\phi)} m_p^{(\phi)}}{K_p^{(\phi)}}} e^{j\frac{2\pi k_p^{(\theta)} m_p^{(\theta)}}{K_p^{(\theta)}}} \tag{7}$$
$$= S(\omega) \sum_{k_p^{(\theta)}=0}^{K_p^{(\theta)}-1} \sum_{k_p^{(\phi)}=0}^{K_p^{(\phi)}-1} e^{j\omega\hat{r}_p\alpha\cos(\theta-\theta_{k_p^{(\theta)}})\cos(\phi-\phi_{k_p^{(\phi)}})} e^{j\frac{2\pi k_p^{(\phi)} m_p^{(\phi)}}{K_p^{(\phi)}}} e^{j\frac{2\pi k_p^{(\theta)} m_p^{(\theta)}}{K_p^{(\theta)}}}.$$

Taking DTFT on both size of equation (6) and using (7), we have

$$y_p(\omega) = \sum_{m_p^{(\theta)}=-L_p^{(\theta)}}^{L_p^{(\theta)}} \sum_{m_p^{(\phi)}=-L_p^{(\phi)}}^{L_p^{(\phi)}} g_{m_p^{(\phi)},m_p^{(\theta)}} V_{m_p^{(\phi)},m_p^{(\theta)}}(\omega) H_{m_p^{(\phi)},m_p^{(\theta)}}(\omega)$$
$$= S(\omega) \sum_{m_p^{(\theta)}=-L_p^{(\theta)}}^{L_p^{(\theta)}} \sum_{m_p^{(\phi)}=-L_p^{(\phi)}}^{L_p^{(\phi)}} g_{m_p^{(\phi)},m_p^{(\theta)}} H_{m_p^{(\phi)},m_p^{(\theta)}}(\omega) \tag{8}$$
$$\cdot \left(\sum_{k_p^{(\theta)}=0}^{K_p^{(\theta)}-1} \sum_{k_p^{(\phi)}=0}^{K_p^{(\phi)}-1} e^{j\omega\hat{r}_p\alpha\cos(\theta-\theta_{k_p^{(\theta)}})\cos(\phi-\phi_{k_p^{(\phi)}})} e^{j\frac{2\pi k_p^{(\phi)} m_p^{(\phi)}}{K_p^{(\phi)}}} e^{j\frac{2\pi k_p^{(\theta)} m_p^{(\theta)}}{K_p^{(\theta)}}} \right).$$

Hence, the spatial-temporal response of the p^{th} ring is

$$G_p(\omega,\phi,\theta) = \sum_{m_p^{(\theta)}=-L_p^{(\theta)}}^{L_p^{(\theta)}} \sum_{m_p^{(\phi)}=-L_p^{(\phi)}}^{L_p^{(\phi)}} g_{m_p^{(\phi)},m_p^{(\theta)}} \{H_{m_p^{(\phi)},m_p^{(\theta)}}(\omega) \tag{9}$$
$$\cdot \sum_{k_p^{(\theta)}=0}^{K_p^{(\theta)}-1} \sum_{k_p^{(\phi)}=0}^{K_p^{(\phi)}-1} e^{j\omega\hat{r}_p\alpha\cos(\theta-\theta_{k_p^{(\theta)}})\cos(\phi-\phi_{k_p^{(\phi)}})} e^{j\frac{2\pi k_p^{(\phi)} m_p^{(\phi)}}{K_p^{(\phi)}}} e^{j\frac{2\pi k_p^{(\theta)} m_p^{(\theta)}}{K_p^{(\theta)}}} \cdot \}$$

To obtain a frequency invariant response, the term inside the brace should be independent of the frequency variable ω. To proceed further, we use the following trigonometric identity

$$\cos(\theta-\theta_{l_p})\cos(\phi-\phi_{k_p}) \tag{10}$$
$$= \tfrac{1}{2}[\cos(\theta-\theta_{k_p^{(\theta)}}+\phi-\phi_{k_p^{(\phi)}}) + \cos(\theta-\theta_{k_p^{(\theta)}}-\phi+\phi_{k_p^{(\phi)}})]$$

and the expansion [16],

$$e^{j\beta\cos\gamma} = \sum_{n=-\infty}^{+\infty} j^n J_n(\beta) e^{jn\gamma}, \tag{11}$$

where $J_n(\beta)$ is the Bessel function of the first kind, to simplify (9). After some manipulation, we get

$$G_p(\omega,\phi,\theta) = \sum_{m_p^{(\theta)}=-L_p^{(\theta)}}^{L_p^{(\theta)}} \sum_{m_p^{(\phi)}=-L_p^{(\phi)}}^{L_p^{(\phi)}} g_{m_p^{(\phi)},m_p^{(\theta)}} \{H_{m_p^{(\phi)},m_p^{(\theta)}}(\omega) \tag{12}$$
$$\cdot \sum_{n=-\infty}^{+\infty} \sum_{m=-\infty}^{+\infty} j^n J_n(\frac{\omega\alpha\hat{r}_p}{2}) j^m J_m(\frac{\omega\alpha\hat{r}_p}{2})$$
$$\cdot (\sum_{k_p^{(\phi)}=0}^{K_p^{(\phi)}-1} e^{j(n-m)\phi} e^{j(\frac{-n+m+m_p^{(\phi)}}{K_p^{(\phi)}})2\pi k_p^{(\phi)}}) (\sum_{k_p^{(\theta)}=0}^{K_p^{(\theta)}-1} e^{j(n+m)\theta} e^{j(\frac{-n-m+m_p^{(\theta)}}{K_p^{(\theta)}})2\pi k_p^{(\theta)}}) \}$$

Further, the term inside the bracket is evaluated to be

$$\sum_{k_p^{(\phi)}=0}^{K_p^{(\phi)}-1} e^{j(\frac{-n+m+m_p^{(\phi)}}{K_p^{(\phi)}})2\pi k_p^{(\phi)}} = \begin{cases} K_p^{(\phi)} & -n+m+m_p^{(\phi)} = K_p^{(\phi)} q \\ 0 & otherwise \end{cases} \tag{13}$$

and $$\sum_{k_p^{(\theta)}=0}^{K_p^{(\theta)}-1} e^{j(\frac{-n-m+m_p^{(\theta)}}{K_p^{(\theta)}})2\pi k_p^{(\theta)}} = \begin{cases} K_p^{(\theta)} & -n-m+m_p^{(\theta)} = K_p^{(\theta)} q \\ 0 & otherwise \end{cases} \tag{14}$$

Substituting (13) and (14) into (12) gives

$$G_p(\omega,\phi,\theta) = \sum_{m_p^{(\theta)}=-L_p^{(\theta)}}^{L_p^{(\theta)}} \sum_{m_p^{(\phi)}=-L_p^{(\phi)}}^{L_p^{(\phi)}} g_{m_p^{(\phi)},m_p^{(\theta)}} \{H_{m_p^{(\phi)},m_p^{(\theta)}}(\omega) \tag{15}$$
$$\cdot K_p^{(\phi)} \sum_{-n+m=K_p^{(\phi)}q-m_p^{(\phi)}} j^n J_n(\frac{\omega\alpha\hat{r}_p}{2}) e^{j(n-m)\phi} \cdot$$
$$\cdot K_p^{(\theta)} \sum_{-n-m=K_p^{(\theta)}q-m_p^{(\theta)}} j^m J_m(\frac{\omega\alpha\hat{r}_p}{2}) e^{j(n+m)\theta} \}$$

From [16], the Bessel function has the following property

$$\left| J_{|n|}(\omega\hat{r}_p\alpha) \right| \le \left(\frac{\omega\hat{r}_p\alpha e}{2|n|} \right)^{|n|}. \tag{16}$$

Therefore, for sufficiently large value of *n*, the value of the Bessel function will be negligibly small. In other words, if the number of sensors is large enough, $G_p(\omega,\phi,\theta)$ can be approximated by

$$G_p(\omega,\phi,\theta) = \sum_{m_p^{(\theta)}=-L_p^{(\theta)}}^{L_p^{(\theta)}} \sum_{m_p^{(\phi)}=-L_p^{(\phi)}}^{L_p^{(\phi)}} g_{m_p^{(\phi)},m_p^{(\theta)}} e^{jm_p^{(\phi)}\phi} e^{jm_p^{(\theta)}\theta} \tag{17}$$
$$\cdot \left[j^{m_p^{(\theta)}} K_p^{(\phi)} K_p^{(\theta)} J_{(m_p^{(\theta)}+m_p^{(\phi)})/2}(\frac{\omega\alpha\hat{r}_p}{2}) J_{(m_p^{(\theta)}-m_p^{(\phi)})/2}(\frac{\omega\alpha\hat{r}_p}{2}) H_{m_p^{(\phi)},m_p^{(\theta)}}(\omega) \right]$$

with $m_p^{(\phi)} + m_p^{(\theta)} = 2n$, n is an integer. It can be seen that for a given radius r_p , the bandwidth of the array, without compensation, is determined by the term $J_{(m_p^{(\theta)}+m_p^{(\phi)})/2}(\omega\alpha\hat{r}_p/2)J_{(m_p^{(\theta)}-m_p^{(\phi)})/2}(\omega\alpha\hat{r}_p/2)$. Rings and hence spheres with small radii usually have better high frequency response and vice versa. Therefore, to obtain a FI-UCSA with large bandwidth, small responses of the Bessel function at certain frequencies have to be compensated by $H_{m_p^{(\phi)},m_p^{(\theta)}}(\omega)$. This is undesirable in general because it leads to considerable noise amplification. Fortunately, by employing more spheres in a UCSA, a wider bandwidth can be obtained.

In a UCSA FIB, the outer spheres have more phase modes than the inner ones. Let the weighting matrices of the rings be identical, i.e. $\boldsymbol{g}_1 = \boldsymbol{g}_2 = \cdots = \boldsymbol{g}_P$, where $\boldsymbol{g}_P$ is the $M_P^{(\phi)} \times M_P^{(\theta)}$ spatial weight matrix with $[\boldsymbol{g}_p]_{m_p^{(\phi)},m_p^{(\theta)}} = g_{m_p^{(\phi)},m_p^{(\theta)}}$. These equalities can be implemented by setting the supplement compensation filters in the inner rings to zeros. The overall response of the beamformer can be written as:

$$G(\omega,\phi,\theta) = \sum_{p=1}^{P} G_p(\omega,\phi,\theta) = \sum_{m^{(\theta)}=-L_p^{(\theta)}}^{L_p^{(\theta)}} \sum_{m^{(\phi)}=-L_p^{(\phi)}}^{L_p^{(\phi)}} g_{m^{(\phi)},m^{(\theta)}} e^{jm^{(\phi)}\phi} e^{jm^{(\theta)}\theta}$$
$$\cdot \sum_{p=1}^{P} j^{m^{(\theta)}} K_p^{(\phi)} K_p^{(\theta)} J_{(m^{(\theta)}+m^{(\phi)})/2}\left(\frac{\omega\alpha\hat{r}_p}{2}\right) J_{(m^{(\theta)}-m^{(\phi)})/2}\left(\frac{\omega\alpha\hat{r}_p}{2}\right) H_{m_p^{(\phi)},m_p^{(\theta)}}(\omega) \tag{18}$$

If the filters $H_{m_p^{(\phi)},m_p^{(\theta)}}(\omega)$ are designed such that

$$\sum_{p=1}^{P} j^{m^{(\theta)}} K_p^{(\phi)} K_p^{(\theta)} H_{m_p^{(\phi)},m_p^{(\theta)}}(\omega) \cdot J_{(m^{(\theta)}+m^{(\phi)})/2}\left(\frac{\omega\alpha\hat{r}_p}{2}\right) J_{(m^{(\theta)}-m^{(\phi)})/2}\left(\frac{\omega\alpha\hat{r}_p}{2}\right) \approx 1 \tag{19}$$
$$, \ \omega \in [\omega_L, \omega_U],$$

where ω_L and ω_U are respectively the lower and upper frequencies of interest, then the beamformer in (19) will be approximately frequency invariant within $\omega \in [\omega_L, \omega_U]$ and

$$G(\omega,\phi,\theta) \approx G(\phi,\theta) = \sum_{m^{(\theta)}=-L_p^{(\theta)}}^{L_p^{(\theta)}} \sum_{m_p^{(\phi)}=-L_p^{(\phi)}}^{L_p^{(\phi)}} g_{m^{(\phi)},m^{(\theta)}} e^{jm^{(\phi)}\phi} e^{jm^{(\theta)}\theta} \tag{20}$$

Furthermore, its far field pattern is now governed by the spatial weighting $\{g_{m^{(\phi)},m^{(\theta)}}\}$ alone. Since the left hand side of (19) is a linear function of the filter coefficients in $H_{m_p^{(\phi)},m_p^{(\theta)}}(\omega)$'s, the design problem in (19) can be treated as a filter design problem with all the filter outputs adding up to a desire response of value 1. If the minimax error criterion is used, the filter coefficients for $H_{m_p^{(\phi)},m_p^{(\theta)}}(\omega)$ can be determined by second order programming (SOCP) [15]. It can also be seen from (20) that the far field spatial response is similar to that of a 2D digital FIR filter with impulse response $\{g_{m^{(\phi)},m^{(\theta)}}\}$. Therefore, $G(\phi,\theta)$ can be designed by conventional 2D filter design algorithms such as window method or SOCP if convex quadratic constraints are to be imposed. In addition, angular shifted versions of (20) can be derived by modulating $\{g_{m^{(\phi)},m^{(\theta)}}\}$ with sinusoids at appropriate frequencies. This property can also be used to generate a set of broadband beamformers uniformly spaced in the angular domain. Further, a broadband beamspace array with equally spaced angles can be readily and efficiently implemented using the basis functions of the DFT. Real-time adaptation of the beam pattern to suppress undesired interference is also simpler than traditional broadband adaptive array using tapped delay lines. We now consider a design example.

IV. Design Example

In this example, a two-sphere UCSA is considered. It is obtained by rotating UCCAs with two rings. The inner ring and the outer ring have $K_1^{(\phi)} = 10$ and $K_2^{(\phi)} = 18$ omnidirectional sensors, respectively. The inner ring and outer ring are then rotated with $K_1^{(\theta)} = 10$, $K_2^{(\theta)} = 18$, respectively. The required bandwidth of the UCSA-FIB is $\omega \in [0.3\pi, 0.7\pi]$. The numbers of phase modes are set as $M_1^{(\phi)} = M_1^{(\theta)} = 9$ and $M_2^{(\phi)} = M_2^{(\theta)} = 17$, We choose the central 9 spatial filter coefficients (phase mode) out of the 17 to shape the spatial response of the UCSA FIB. The desired beam is targeted at $(\phi,\theta) = (0^o, 0^o)$ and the beamwidth is 10^o . Separable spatial weights $\{g_{m^{(\phi)},m^{(\theta)}}\}$ are employed here for low complexity. They are obtained from two one-dimensional spatial weights that were designed by the Parks-McClellan algorithm according to the given specification with the same passband and stopband ripples. The perspective views of the frequency responses against azimuth and elevation angles are shown in figures 5 and 6, respectively. The FI performance is very satisfactory. To illustrate the FI performance more clearly, the frequency responses of the UCSA-FIB for $\omega \in [0.3\pi, 0.7\pi]$ are overlapped together in Figure 7. The frequency response is seen to be approximately FI, with deep nulls formed at the desired position over the bandwidth of interest. Figure 8 shows the contour of the 2D spatial response of the UCSA-FIB at the frequency $\omega = 0.5\pi$. The spatial responses at other frequencies of interest are almost the same due to the FI characteristic of the beamformer and are not plotted here. Like their FI-UCCA counterparts [12] [13], the above FIB can be modulated to form a bank of FIBs for broadband DOA estimation. Moreover, the weights $\{g_{m^{(\phi)},m^{(\theta)}}\}$ can be made adaptive to form adaptive UCSA-FIB with very few variable multipliers and fast convergence speed. Due to page limitation, the details will be reported in future publications.

V. Conclusions

The theory and design of uniform concentric spherical array (UCSA) having nearly frequency invariant (FI) characteristics are presented. By compensating the frequency dependency of individual phase modes using a digital beamforming network, the far field pattern of the array is found to be determined by a set of weights and it is approximately invariant over a wide range of frequencies. Compared with FI uniform concentric circular array (UCCA), FI UCSA is able to electronically steer in both the azimuth and elevation angles. The FI and 2D electronically steerable characteristics of the UCSA-FIB are illustrated by a design example.

References

[1] D. H. Johnson and D. E. Dudgeon, *Array signal processing: concepts and techniques*, Prentice Hall, 1993.

[2] H. Krim and M. Viberg, "Two decades of array signal processing research: the parametric approach," *IEEE Signal Processing Mag.*, vol. 13, pp. 67-94, Jul. 1996.

[3] B. D. Van Veen and K. M. Buckley, "Beamforming: a versatile approach to spatial filtering," *IEEE ASSP Mag.*, vol. 52, pp. 4-24, Apr. 1988.

[4] T. Sekiguchi and Y. Karasawa, "Wideband beamspace adaptive array utilizing FIR Fan filters for multibeam forming," *IEEE Trans. Signal Processing*, vol. 48, pp. 277-284, Jan. 2000.

[5] D. B. Ward, R. A. Kennedy and R. C. Williamson, "Theory and design of broadband sensor arrays with frequency invariant far-field

beam patterns," *J. Acoust. Soc. Amer.*, vol. 97, no.2, pp.1023-1034, Feb. 1995.

[6] D. B. Ward, R. A. Kennedy and R. C. Williamson, "FIR filter design for frequency invariant beamformers," *IEEE Signal Processing Lett.*, vol.3, pp. 69-71, Mar. 2000.

[7] M. Ghavami and R. Kohno, "Recursive fan filters for a broad-band partially adaptive antenna," *IEEE Trans. Commun.*, vol. 48, pp.185-188, Feb. 2000.

[8] D. B. Ward, Z. Ding and R. A. Kennedy, "Broadband DOA estimation using frequency invariant beamforming," *IEEE Trans. Signal Processing*, vol. 46, pp. 1463-1469, May 1998.

[9] R. O. Schmidt, "Multiple emitter location and signal parameter estimation," *IEEE Trans. Antennas Propagat.*, vol. AP-34, pp. 276-280, Mar. 1986.

[10] H. Steyskal, "Circular array with frequency-invariant pattern," *Antennas and Propagation Society International Symposium 1989*, AP-S. Digest, vol. 3, pg. 1477-1480, 1989.

[11] S. C. Chan and Carson K. S. Pun, "On the design of digital broadband beamformer for uniform circular array with frequency invariant characteristics," *IEEE ISCAS2002*, vol. 1, pp. 693-696, May 2002.

[12] S. C. Chan and H. H. Chen, "Theory and design of uniform concentric circular Arrays with frequency invariant characteristics", *IEEE ICASSP'05*, vol. 4, pp. 805-808, Mar. 2005.

[13] S. C. Chan, H. H. Chen and K. L. Ho, "Adaptive beamforming using uniform concentric circular arrays with frequency invariant characteristics", *IEEE ISCAS'05*, pp. 4321- 4324, May 2005.

[14] J. O. Coleman and D. P. Scholnik, "Design of nonlinear phase FIR Filters with second-order cone programming," in *Proc. IEEE MWSCAS*, vol. 1, pp. 409-412, 1999.

[15] M. S. Lobo, L. Vandenberghe, S. Boyd and H. Lebret, "Applications of second-order cone programming", *Linear Algebra Application*, vol. 248, pp.193-228, Nov. 1998.

[16] M. Abramowitz and I. A. Stegun, *Handbook of Mathematical Functions*, New York: Dover, 1965.

FIGURES

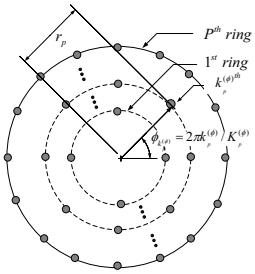

Figure 1. A UCCA with P rings and K_p sensors at each ring.

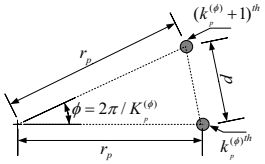

Figure 2. Relationship between inter-sensor spacing and the radius of the p^{th} ring of the UCCA.

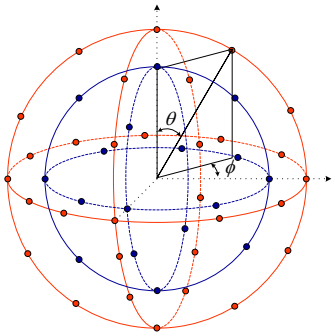

Figure 3. Geometry of the UCSA.

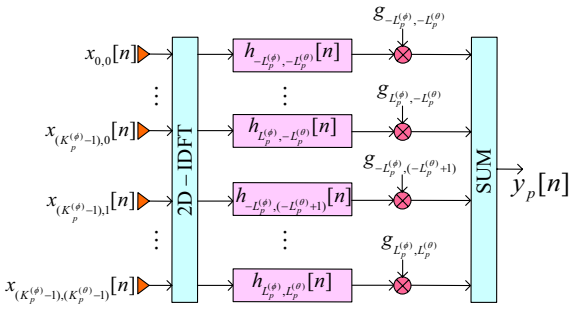

Figure 4. UCSA-FIB block diagram for the p^{th} sphere.

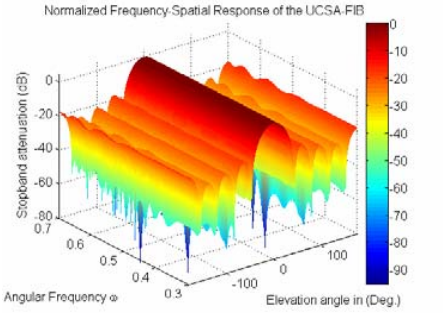

Figure 5. Frequency responses against azimuth angles.

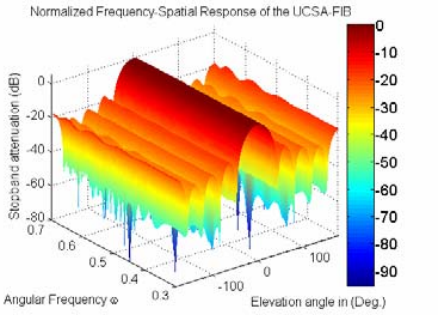

Figure 6. Frequency responses against elevation angles.

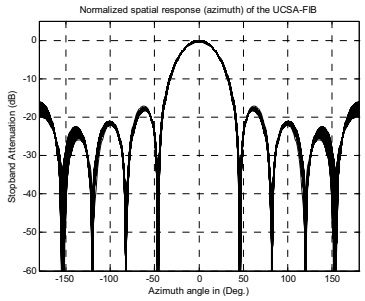

Figure 7. Spatial response of the UCSA-FIB in azimuth angle.

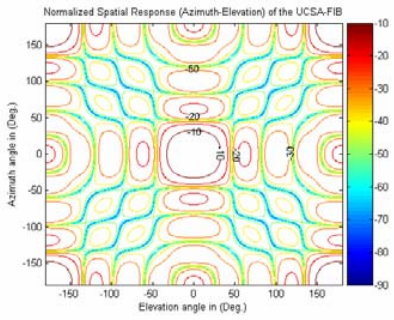

Figure 8. Spatial responses of the UCSA-FIB.